AIMS Materials Science, 5(3): 543–550.
DOI: 10.3934/matersci.2018.3.543
Received: 05 April 2018
Accepted: 31 May 2018
Published: 11 June 2018

http://www.aimspress.com/journal/Materials

Research article

Formation of $(Cu)_n$ & $(Cu_2O)_n$ nanostructures with the stability of their clusters

Kulpash Iskakova[1,*], Rif Akhmaltdinov[1] and Temirgali Kuketaev[2]

[1] Department of Physics and Mathematics, Kazakh National Pedagogical University, Almaty, Kazakhstan
[2] Department of Physics and Technics, Karaganda State University, Karaganda, Kazakhstan

*** Correspondence:** Email: ahmanovakulpash@yahoo.com.

Abstract: We investigated the electronic structure and the properties of cupper (Cu) and compound semiconductor (Cu_2O) by with the help of computer simulation of the programs developed by us and obtaining various morphologies and properties of Cu nanostructures by the method of template synthesis, including the study of the direction of formation processes and the practical application of ion tracks. In calculations of the computer simulation programs developed by us, the general and area-predicted density of states and the band dispersion of optimized crystal structures with different structural units $(Cu)_n$ (n = 6, 12) and $(Cu_2O)_n$ (n = 16, 23) were described. Accordingly, this leads to the prediction that $(Cu)_n$ at n = 12 and $(Cu_2O)_n$ at n = 23 take a high electron density, and that the energy maximum points arise where there is a low electron density and, conversely, for electron energy minima, the electron density is high. The maxima of the level energy n = 2 for $(Cu)_n$ and $(Cu_2O)_n$, the corresponding electron densities also reached their maximums, but these values of the metallic and semiconductor junctions, respectively, were sharply different in value when compared with each other. This indicates that the changes in the electronic states were due mainly to the replacement of the oxygen atom and subsequent modification of the crystalline field.

Keywords: BCC structure; FCC structure; clusters; direct space; inverse space; lattice

1. Introduction

The production of metallic and semiconductor nanotubes by various methods is becoming increasingly important. Modern methods used to design ultra-thin tubes include: spin coating and

injection molding, thermal deposition, step-by-step assembly, chemical self-assembly, various computer simulation techniques. Of particular importance is the computer simulation of various nanostructures, on which the greater part of the technology for obtaining nanocrystalline materials depends. At the same time, it should be noted that the structure and properties of nanocrystalline materials in computer simulation depend on different sets of given initial modeling parameters.

The study of the structures and geometry of neutral and charged atomic clusters uses different methods: the non-empirical Hartree-Fock method (HF) and the second-order Möller-Plesset method. To study the dependence of the composition on the physical properties of small and medium clusters, a combination of the first principles of computing electronic structures and semiempirical methods is used. The process of cluster formation in a nanostructure is accompanied by a discontinuity of symmetry, which can be identified according to the specific structure of the cluster [1]. For clusters of several atoms (~5) molecular dynamics based on semi-empirical methods (MOPAC PM3) was used before the quantum-mechanical calculation.

Semiconductor crystal calculations are carried out using the projector method of the coupled wave of the plane wave pseudopotential and the generalized gradient approximation (GGA) for the exchange-correlation energy. Geometric optimization and preliminary calculations are performed using the GAUSSIAN package of various versions with a basic function set and the core electronic effective core potential (EPO) ECP10MDF35 [2–8].

As shown by the analysis of literature data, a so-called template synthesis, which includes the direction of studying the processes of formation and practical application of ion tracks, is assigned a special place among the methods currently being developed among methods of obtaining various morphologies and properties of nanostructures in solids. This technique is based on a unique phenomenon when high-energy heavy ions induce a very narrow latent track containing a highly disordered zone with a diameter of about 5–10 nm [9–12].

2. Materials and method

In the calculation method used, the results are shown in three-dimensional reciprocal space, and the summary data are given in the corresponding tables. The calculations were carried out using the screening method of the pseudo potential and finding the polynomial solution of the Schrödinger equation for the energy in the space of wave vectors. A polynomial solution for energy is taken such that it fits up to several eV, depending on the system. Nanoparticles are placed in a cube with concave sides up to 20 Å with periodic boundary conditions. The atomic structure is completely idealized without any deviations, while the absolute value of the force acting on each ion becomes less than 0.005 eV/Å and the energy as a result converges within an error of 0.0001 eV. Integration of the Brillouin zone is performed using only the point *G*. The configurations of the valence electrons for $(Cu)_n$ are chosen so that the state s^2p^1 (s^2p^3) is present.

3. Results

Figure 1a shows the optimized structure of a cell with one electron $(Cu)_n$ with n = 6, 12. Table 1 shows the calculated electron density [13] in the interspheral space, the electron avulsion of the highest occupied atomic orbital level and the transition to the lowest free interspheral space and the energy difference empty and three-dimensional filled cells of $(Cu)_n$ nanoparticles. Figure 1b shows

the electron density values, listed in Table 1. For n = 12, the cell occupied by an electron has a high stability with cubic symmetry (as for Cu_2O), which is shown in Figure 2 [14–16] (We also have a spontaneous ordering, but with Cu_2O. See also for GaAs [17–20]). There are two types of coupling, namely, the short-range exchange coupling (1.87 Å) of hexagonal bonds, which have a binding character sp^2 to a greater extent, and the exchange of relatively long-acting (1.95 Å) bonds of a hexagon with a rhombus having the nature of the sp^3 bonds. The variation of valence angles and bond lengths for various metal-gas compounds appears. It is found that the cells of copper–oxygen nanoparticles are more concave because of the strong character of sp^3 compared to the $(Cu)_n$ cells, as can be clearly seen from the comparison of the Cu_2O cell in Figure 2a with the cell $(Cu)_n$ in Figure 1. The first is more concave.

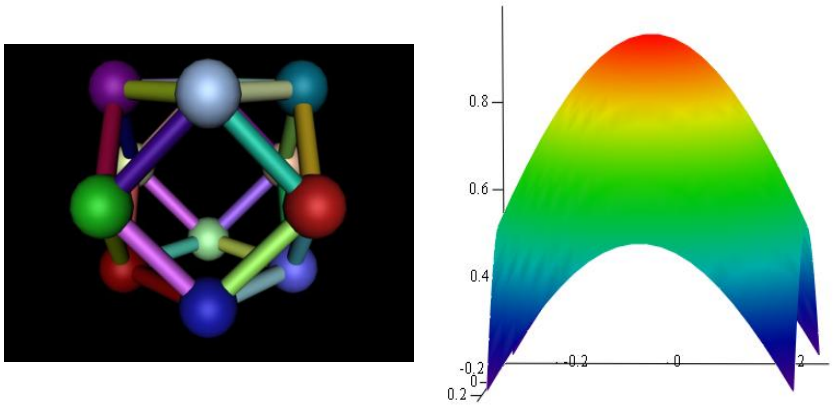

(a) (b)

Figure 1. (a) The optimized structure of a cell with one electron $(Cu)_n$ n = 12; (b) the electron density in the interspheral space of a cell with one electron $(Cu)_n$ n = 12.

Table 1. The electron density in the interspheral space of a cell with one electron $(Cu)_n$ n = 12.

k_x, Å	k_y, Å	ρ, Å^{-2}
−0.276	−0.276	0.225
−0.246	−0.246	0.414
−0.236	−0.236	0.534
−0.226	−0.226	0.561
−0.216	−0.216	0.489
−0.206	−0.206	0.333
−0.196	−0.196	0.414
−0.186	−0.186	0.636
0.186	0.186	0.775
0.196	0.196	0.806
0.206	0.206	0.723
0.216	0.216	0.541
0.226	0.226	0.534
0.236	0.236	0.775
0.246	0.246	0.926
0.276	0.276	0.959

For $(Cu)_n$ and Cu_2O, the three-dimensional filled cell with respect to the electron density lies higher than the empty one [21], and so all the nanoparticles of the metal and semiconductor-cuprite with n = 16 indicate in favor of the empty cell of the structure (Figure 2a), but the energy difference between empty and filled cells decreases (see also Table 2).

Cu_2O has a full filled shell, so that it is impossible the existence of the phase instability for the charge transferring. X-ray phase analysis of Cu_2O films obtained by chemical deposition showed an identity with a single-phase composition of polycrystalline cuprous oxide Cu_2O obtained by high-temperature oxidation. On the other hand, in the three-dimensional filled cell $(Cu)_n$ and $(Cu_2O)_n$, as shown in Figure 2b, the positions of all the peaks are preserved, but their intensities have sharply decreased. The most intense intensity peaks of $(Cu)_n$ were of the order of $\rho = 10^{27}$–10^{31}, and for $(Cu_2O)_n$, they were 1–1.5. The difference between the energies $(Cu)_n$ between the filled cells n = 6 and 12 is, however, only 0.186 eV. In the interspheral space $(Cu_2O)_n$ n = 16 in the filled cells, there are two oxygen atoms inside the cell that is bent with a more sp^3-binding character. Central ions O and Cu_2 bind well in a cell with two 2 ions of O, in the cell, the O ions are optimally connected [13]. Here $(Cu_2O)_n$ also has the largest discontinuity from the uniform increasing of nanoparticles and the optimality decreases for these limits (see Figure 3 and Table 3).

The structure of the $(Cu)_n$ cell with n = 6 and 12 shows an important sp^2 bond with less deformed ones (see Figure 1 for $(Cu)_n$), analogous to cells n = 16 and 23 for $(Cu_2O)_n$. However, for $(Cu)_n$ and $(Cu_2O)_n$, empty cells are deformed more and develop a more significant bond sp^3. This is why filling the cell is more appropriate in these cases, as shown in Figure 2. There is a large decrease in the electron density ρ (see the Table 3) for n = 23, and this shows that the tendency of the structure of the filled cell becomes much stronger than the case of n = 16.

Thus, for n = 12, an increase in the electron density and an energy decrease of 0.1 eV for $(Cu)_{12}$ arise in a three-dimensional filled cell. Moreover, $(Cu_2O)_{16}$ shows a remarkable transition to the three-dimensional structure of a filled cell with the highest electronic density ρ $(Cu_2O)_{23}$ and a large discontinuity in the exchange bonds of lengths 1.87, 1.90, and 1.92 Å compared to n = 16.

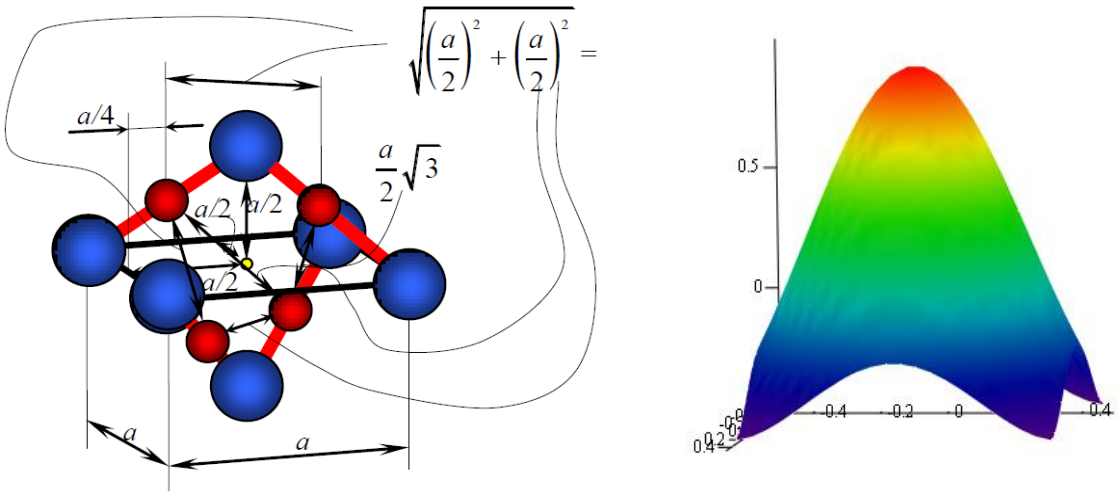

(a) (b)

Figure 2. (a) Interspheral space cell of Cu_2O; (b) the electron density in the $(Cu_2O)_n$ interspheral space cell.

Table 2. The electron density in the $(Cu_2O)_n$ interspheral space cell.

k_x, Å	k_y, Å	ρ, Å^{-2}
−0.468	−0.468	−0.447
−0.458	−0.458	−0.448
−0.448	−0.448	−0.392
−0.438	−0.438	−0.323
−0.428	−0.428	−0.255
−0.418	−0.418	−0.2
−0.408	−0.408	−0.167
−0.398	−0.398	−0.162
0.398	0.398	−0.184
0.408	0.408	−0.232
0.418	0.418	−0.296
0.428	0.428	−0.366
0.438	0.438	−0.429
0.448	0.448	−0.47
0.458	0.458	−0.448
0.468	0.468	−0.377

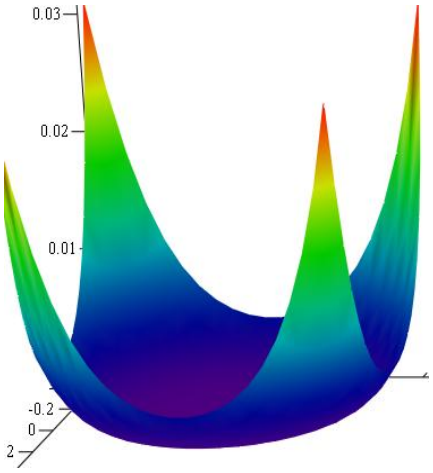

Figure 3. The electron energy in the $(Cu_2O)_n$ interspheral space cell.

Table 3. The electron energy in the $(Cu_2O)_n$ interspheral space cell.

k_x, Å	k_y, Å	E, eV
−0.468	−0.468	0.133
−0.458	−0.458	0.06
−0.448	−0.448	0.028
−0.438	−0.438	0.015
−0.428	−0.428	0.01
−0.418	−0.418	9.465×10^{-3}

Continued on next page

k_x, Å	k_y, Å	E, eV
−0.408	−0.408	0.012
−0.398	−0.398	0.022
0.398	0.398	0.045
0.408	0.408	0.099
0.418	0.418	0.06
0.428	0.428	0.021
0.438	0.438	7.54
0.448	0.448	3×10^{-3}
0.458	0.458	1.627×10^{-3}
0.468	0.468	1.463×10^{-3}

4. Discussion

Using the modeling method described above, we obtain the geometry of Cu nanotubes. The results of the simulation of Cu nanotubes gave their dimensions with averaged dimensions of 10 μm in height, 378 nm in outer diameter, 181 nm in internal diameter, and a wall thickness of about 101 nm. The elemental composition of such nanotubes is 95–98% composed of Cu and 2–5% oxygen. Nanotubes obtained by chemical synthesis correspond to the predicted geometric characteristics (see Figure 4). Energy-dispersive analysis was used to determine the elemental composition of Cu nanotubes.

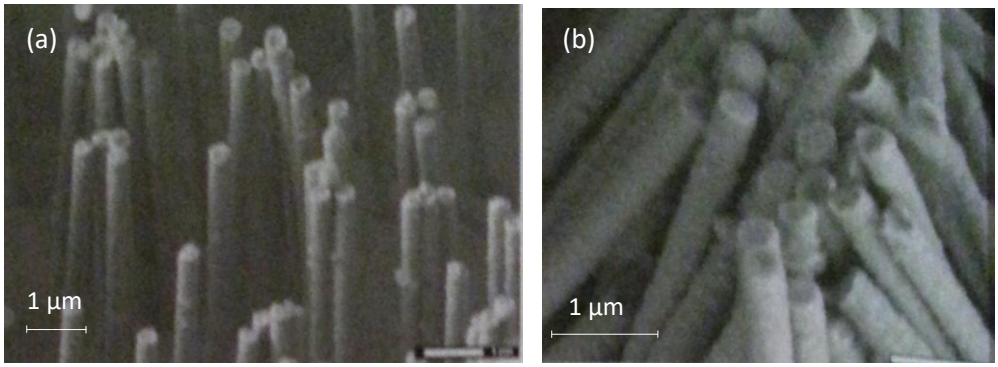

Figure 4. The nanotubes of Cu.

Electrodes for electro-chemical operations are aluminum or copper. In the course of experiments with Cu_2O, it becomes possible to grow such nanotubes.

5. Conclusions

The electron density and the energy include a number of peaks, which corresponds to the transition of the electron to the interspheral space in the cluster. This minimum binding energy corresponds also to the infinite energy of the electron. The peaks are associated with the transition of the electron to the excited neutral state of the cluster, processes of electrons transition from certain shells to the interspheral space.

Conflict of interest

The authors declare that there is no conflict of interest regarding the publication of this paper.

References

1. Koiller B, Davidovich MAM (1990) Small-crystal approach to ordered semiconductor compounds. *Phys Rev Lett* 41: 3670.
2. Kaur P, Sekhon SS, Kumar V (2012) Empty cage to three-dimensional structural transition in nanoparticles of III–V compound semiconductors: The finding of magic $(AlP)_{13}$ and $(GaP)_{32}$. *Phys Rev B* 85: 085429.
3. Karamanis P, Pouchan C, Weatherford CA, et al. (2011) Evolution of properties in prolate $(GaAs)_n$ clusters. *J Phys Chem C* 115: 97–107.
4. Malloci G, Chiodo L, Rubio A, et al. (2012) Structural and optoelectronic properties of unsaturated ZnO and ZnS nanoclusters. *J Phys Chem C* 116: 8741–8746.
5. Kwong HH, Feng YP, Boo TB (2001) Composition dependent properties of GaAs clusters. *Comput Phys Commun* 142: 290–294.
6. Yang JS, Li BX, Zhan SC (2006) Study of GaAs cluster ions using FP-LMTO MD method. *Phys Lett A* 348: 416–423.
7. Karthikeyan S, Deepika E, Murugan P (2012) Structural Stability and Electronic Properties of CdS Condensed Clusters. *J Phys Chem C* 116: 5981–5985.
8. Musa NM, Isa ARM, Kasmin MK (2008) Structures and bandgaps of small range gallium arsenide nanocluster. *Malays J Fund Appl Sci* 4: 451–455.
9. Deiss E, Holzer F, Haas O (2002) Modeling of an electrically rechargeable alkaline Zn–air battery. *Electrochim Acta* 47: 3995–4010.
10. Lee J, Lee P, Lee H, et al. (2012) Very long Ag nanowire synthesis and its application in a highly transparent, conductive and flexible metal electrode touch panel. *Nanoscale* 4: 6408–6414.
11. Chang CM, Wei CM, Chen SP (2000) Self-diffusion of small clusters on fcc metal (111) surfaces. *Phys Rev Lett* 85: 1044.
12. Chen Z, Shan Z, Li S, et al. (2004) A novel and simple growth route towards ultra-fine ZnO nanowires. *J Cryst Growth* 265: 482–486.
13. Jolk A, Klingshirn CF (1998) Linear and nonlinear excitonic absorption and photoluminescence spectra in Cu_2O: Line shape analysis and exciton drift. *Phys Status Solidi B* 206: 841–850.
14. Muller E, Patterson BD, Spontaneous Ordering in AlGaAs, PSI annual report, 2000. Available from: www.physik.unizh.ch/reports/report2000.html.
15. Patterson BD, Spontaneous Ordering in AlGaAs, PSI annual report, 1997. Available from: www.physik.unizh.ch/reports/report1999.html.
16. Iskakova K, Akhmaltdinov R (2011) Modeling and calculation of the dynamic three-dimensional A^3B^5 models on the example of GaAs. *Int J Appl Phys Math* 1: 112.
17. Iskakova K, Akhmaltdinov R (2012) Modeling and calculation of the algorithm structure of compound semiconductor-type A^3B^5. *Appl Mech Mater* 110–116: 2854–2858.
18. Iskakova K, Akhmaltdinov R (2012) Modeling of the crystal structure growth process of GaAs. *Appl Phys A-Mater* 109: 857–864.

19. Iskakova K, Akhmaltdinov R, Amanova A (2014) The ideal “defects” of the crystal structure of GaAs. *Adv Mater Res* 936: 577–584.
20. Jensen F, Besenbacher F, Lægsgaard E, et al. (1991) Oxidation of Cu(111): two new oxygen induced reconstructions. *Surf Sci* 259: L774–L780.
21. Zunger A (1997) Spontaneous atomic ordering in semiconductor alloys: Causes, carriers, and consequences. *MRS Bull* 22: 20–26.

AIMS Press

© 2018 the Author(s), licensee AIMS Press. This is an open access article distributed under the terms of the Creative Commons Attribution License (http://creativecommons.org/licenses/by/4.0)